JOURNAL OF MATERIALS SCIENCE 33 (1998) 4657–4663

An STM and atomic force microscopy study of the effects of 1.8 MeV electron bombardment on the surface of graphite

Y. J. CHEN, I. H. WILSON, J. B. XU
Department of Electronic Engineering and Materials Technology Research Centre, The Chinese University of Hong Kong, Shatin, N. T., Hong Kong
LIN LIBIN
Department of Physics, Sichuan University, Chengdu 610064, People's Republic of China

Highly oriented pyrolitic graphite was irradiated with 1.8 MeV electrons at 45° and near-grazing (86°) angles of incidence. For doses up to 10^{16} cm^{-2} electrons the surface of the samples subjected to 45° incidence, observed by both STM and atomic force microscopy (AFM) remained the same as the original sample showing only the usual periodic atomic corrugation, with an atomic spacing of 0.246 nm. For near-grazing incidence, at a dose of 5×10^{12} cm^{-2} electrons, features of nanometre size are observed, some elongated along the direction of the beam incidence. These are attributed to the effects of single electron–carbon interactions in the top surface layers. At a dose of 5×10^{14} cm^{-2} electrons (near grazing incidence) both STM and AFM observations show an anomalously large (period 2.5–17 nm) superperiodicity superimposed on the normal 0.246 nm atomic spacing of graphite. This Moiré-like pattern suggests that the corrugations are electronic as well as topographic in origin. We propose that near-grazing incidence electron irradiation causes break-up of the surface layers into fragments, largely retaining six-fold atomic rings, that rotate by a small angle resulting in the observed pattern due to interaction with deeper bulk-structure layers.

1. Introduction

The understanding of particle–solid interactions has arrived at the atomic-scale level with the advent of scanning probe microscopy (SPM). Highly oriented pyrolytic graphite (HOPG) is most often chosen because of its inertness in air and the ease with which it can be cleaved to obtain atomic resolution. The effects of ion bombardment on a HOPG surface, especially single ion impacts, have been extensively studied [1–18]. No matter what ion species are used at energies from 50 eV to 3 GeV and different angles of incidence, nanometre-sized bumps (or hillocks, protrusions, blisters, etc.) are generally observed and are attributed to defects created by atomic displacements. The appearance of these nanometre-sized bumps was considered as the initial stage of volume expansion by high dose ion implantation [19]. However, there is still some controversy regarding the origin of the nanometre-sized structures. The effects of electron bombardment on a solid surface following SEPM analysis have never been reported to our knowledge, since electrons have much lighter mass and much deeper penetration into target materials than ions. Therefore, structural and microstructural changes accompanying electron irradiation usually occur well away from the surface. In this experiment, high energy electrons at near grazing angle of incidence were used to bombard HOPG, and the effects of electron bombardment at the surface are observed using SPM.

2. Experimental procedure

Each sample ($5 \times 5 \times 1$ mm) of HOPG (supplied by NT-MDT Corp. Moscow; ZYB quality standard) was checked by STM before irradiation. All showed atomically flat surfaces with the usual periodic atomic corrugation, with an atomic spacing of 0.246 nm. The 1.8 MeV electron bombardment was conducted by the scanning method at room temperature (10 °C) on an electrostatic accelerator (type: JJ-2). A low beam current ($<0.1\,\mu$A or 1.6×10^{12} cm^{-2} s^{-1}) was used to avoid raising of the temperature, which is estimated to be less than 1°C. The different doses and angles of incidence (relative to the surface normal) used for each sample are shown in Table I. STM and atomic force microscopy (AFM) observations were made in air at ambient temperature with a Nanoscope III SPM system (Digital Instruments, Santa Barbara, CA). The STM, with scanning head A, was operated in both constant height mode (current mode) and constant current mode (height mode). Mechanically cut Pt–Ir wires were used for the STM tip. The tip bias and

TABLE I Doses and angles of incidence applied to samples

Samples	Angles of incidence (deg)	Doses ($e^- cm^{-2}$)
A	86	5×10^{12}
B	86	5×10^{14}
C	45	5×10^{12}
D	45	10^{16}

tunnelling setpoint were 50–80 mV and 1.2–2.0 nA, respectively. Both piezo heads J and A, with a standard Si_3N_4 cantilever, were used for AFM observations. The AFM was operated in constant contact force mode (height mode) for a large scan size and both height and deflection modes for the small scan size, with the force set at 10 nN.

3. Results

Typical STM images for samples C (irradiated with $5 \times 10^{12} e^- cm^{-2}$ at 45°) and D (irradiated with $10^{16} e^- cm^{-2}$ at 45°) are shown in Fig. 1. Large-scan topography (Fig. 1a) shows some flat steps, which can range from a single graphite monolayer to several layers high. At higher magnification (Fig. 1b), atomic resolution is obtained. The appearance was the same as for the original surface: only every other surface carbon atom appears as a protrusion in the STM image with a periodicity of 0.246 ± 0.02 nm and a corrugation of 0.08–0.12 nm. The AFM observations are in good agreement with the STM results.

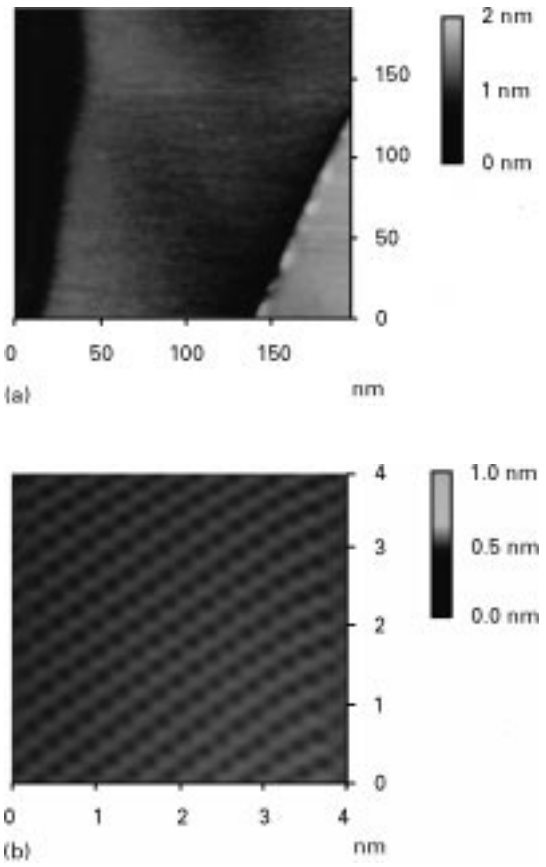

Figure 1 Typical STM image for samples C and D. (a) Height mode large-scan size ($198 \times 198 nm^2$). *Z* range: 2 nm, setpoint: 1.47 nA; bias 65.22 mV; scan rate: 3.82 Hz. The steps are monolayer high. (b) Height mode small-scan size ($4 \times 4 nm^2$). *Z* range: 1 nm; setpoint: 1.24 nA; bias: 64.53 mV; scan rate: 122 Hz. The periodicity of atomic lattice is 0.246 nm with corrugation of 0.08 nm.

For sample A (irradiated with $5 \times 10^{12} e^- cm^{-2}$ at 86°), defects of nanometre scale features are found at some locations, as shown in Fig. 2. The areas in Fig. 2a–d represent 87×87, 100×100, 50×50 and 91×91 nm, respectively. The height mode STM images show hillocks of irregular shape on originally flat surfaces. The height of these hillocks is measured to be 0.2–0.8 nm, with the size ranging from 10 to 600 nm^2. Fig. 2d shows a chain of hillocks, which is about 97 nm long, along the direction of beam incidence. The current mode STM image in Fig. 3 clearly shows that the hillocks are seperated by flat terraces on which normal atomic resolution can be obtained. The graphite lattice appears distorted in the immediate region of the hillocks, with graphite lattice around the hillocks being unperturbed. While these defects can be found at some locations, STM observations at other places show no such features, showing only flat terraces similar to Fig. 1. This means the possibility of observing such defects (every three out of 200 locations showing nanometre-size bumps) is much lower than the density of electrons into the surface, which is the dose ($5 \times 10^{12} e^- cm^{-2}$) divided by a factor of $(\cos 86°)^{-1}$.

For sample B (irradiated with $5 \times 10^{14} e^- cm^{-2}$ at 86°), large-scale periodic features, like two-dimensional waves or rotational Moiré patterns, were observed by STM as shown in Figs 4 and 5. In Fig. 4a, a smooth graphite terrace is seen at the top right-hand corner, while patches of waves can also be seen. Several scans with different offsets were used to determine that the wave field of this wave structure was nearly 600 nm in maximum dimension. Fig. 4b–d shows a higher magnification of a part of the same region as in Fig. 4a. By using Fast Fourier Transform (FFT) analysis, the spacings of the wave pattern are 5.2, 3.7 and 5.9 nm along the three main directions (axes) and the angles between the axes are 103, 123 and 134°, therefore the pattern is approximately hexagonal arrangement but with some distortion. The corrugation is measured to be 0.4 nm, five times larger than the amplitude of the normal atomic corrugation. The current mode STM images in Fig. 4c, d, show large-scale periodicity as well as graphite atomic features. Further inspection of Fig. 4c, d reveals that there is an orientational difference between the atomic lattice and the wave lattice. Atomic lattice images and larger scale wave images were used together to determine this difference and it was found to be 27 ± 3°. The angle between the unit cell directions of the atomic lattice and wave lattice (Moiré relative to graphite fringes) was measured to be 91.6°, therefore the misorientation angle between the graphite lattices of spacing 0.246 nm is 3.2°.

Fig. 5 shows height mode STM images of another large-scale periodic wave feature at different magnifications. Fig. 5a shows a patch of waves (300 nm in maximum dimension) between two smooth graphite terraces. The boundary of the two-dimensional region at the bottom left-hand corner is sharp, while the boundary at the other side exhibits extra structure on

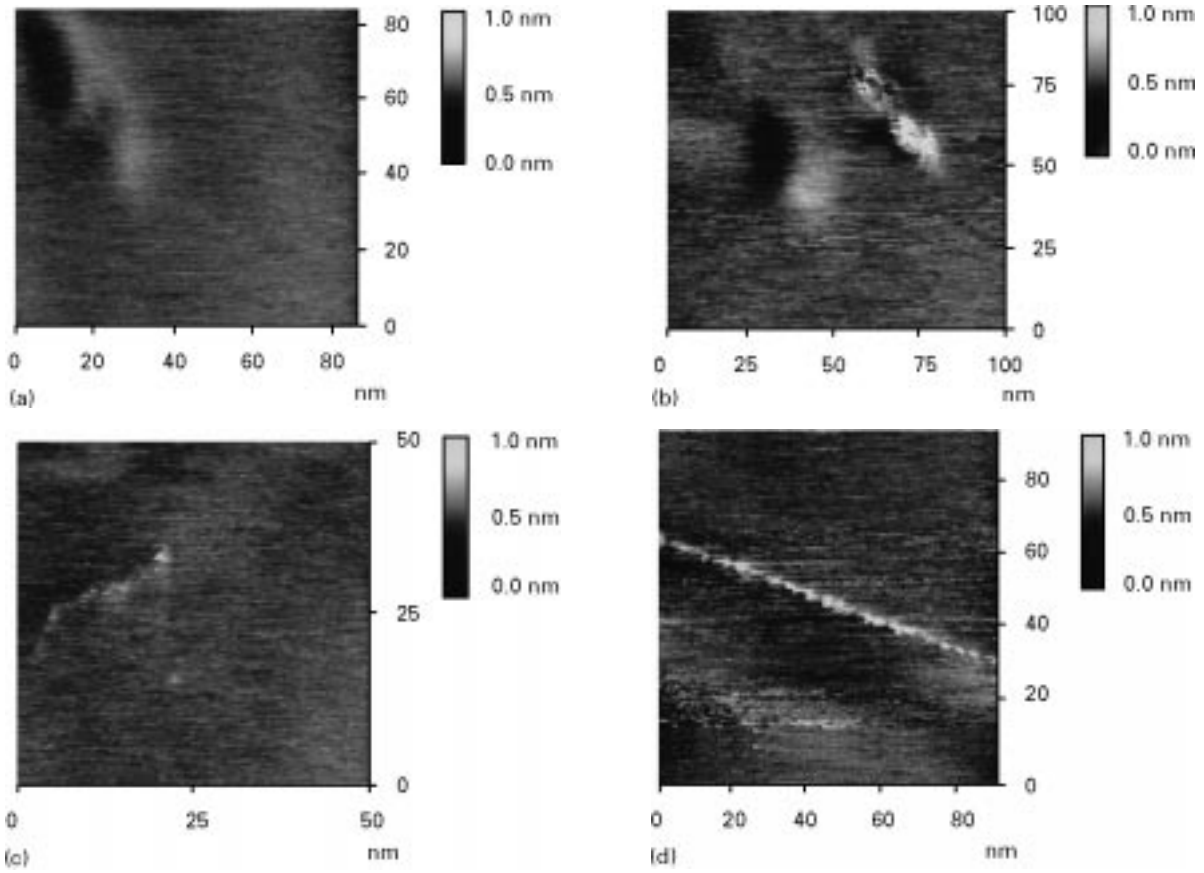

Figure 2 Height mode STM images for sample A. *Z* range: 1 nm; setpoint: 1.81 nA; bias: 56.63 mV. (a) $87 \times 87\ nm^2$ (2.11 Hz) (b) $100 \times 100\ nm^2$ (4.07 Hz) (c) $50 \times 50\ nm^2$ (1.81 Hz), (d). $91 \times 91\ nm^2$ (3.05 Hz). The heights and areas of the hillocks are 0.2–0.8 and 10–600 nm^2. The values in parentheses are scan rates.

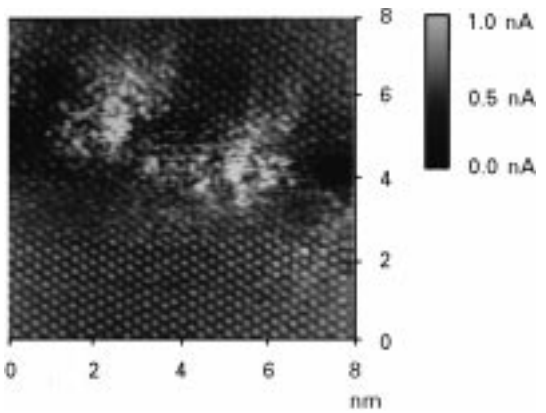

Figure 3 A current mode STM image ($8 \times 8\ nm^2$) for sample A. *Z* range: 1 nm; setpoint: 1.81 nA; bias 56.63 mV; scan rate: 61 Hz.

individual wave peaks. FFT analysis gives the main spacings of 8.5, 7.9 and 9.8 nm, and angles between the axes of 115, 121 and 124°. It also has an approximately hexagonal symmetry. Following the methods used above, the orientational difference between the atomic lattice and the wave lattice is measured to be $25 \pm 2°$, while the misorientation angle between the graphite atomic lattices is measured to be 2°. At the highest magnification (Fig. 5d), the usual graphite atomic corrugation (0.05 nm) is seen, as well as the anomalous contrast (0.38 nm).

These features are also observed in other regions of sample B, though not in all regions (some only show flat terraces as in Fig. 1). By measuring eight such wave features (150–600 nm in maximum dimension, with the amplitude of the giant corrugation of 0.1–0.5 nm), the superperiodicity ranges from 2.5 to 17 nm with rotational misorientation angles of 0.6–5°. This means that the wave features at different locations are different and therefore the irradiated graphite surface is not uniform. In an attempt to corroborate these results, three additional experiments were conducted.

The experimental parameters, such as bias, setpoint, number of pixels, etc., were changed intentionally during STM observation. It was found that wave features images were observable with a setpoint ranging from 80 pA to 3 nA and with both negative and positive bias over the range -500 to $+500$ mV, and the contrast was insensitive to the bias polarity. Images with 128×128, 256×256 and 512×512 pixels showed the same features, which meant that the large superperiodicity was not due to periodic sampling of the graphite atomic lattice. Scans at 27 random locations were completed on the surface of sample B, three locations showed wave features. We cannot estimate the percentage of the coverage of the wave features among the whole area of the surface due to the limitation of the scan dimension.

Both AFM and scanning electron microscopy (SEM) are also used to observe these features. Generally it is more difficult for AFM to measure the superiodicity. Fig. 6a shows a large scan ($1 \times 1\ \mu m$)

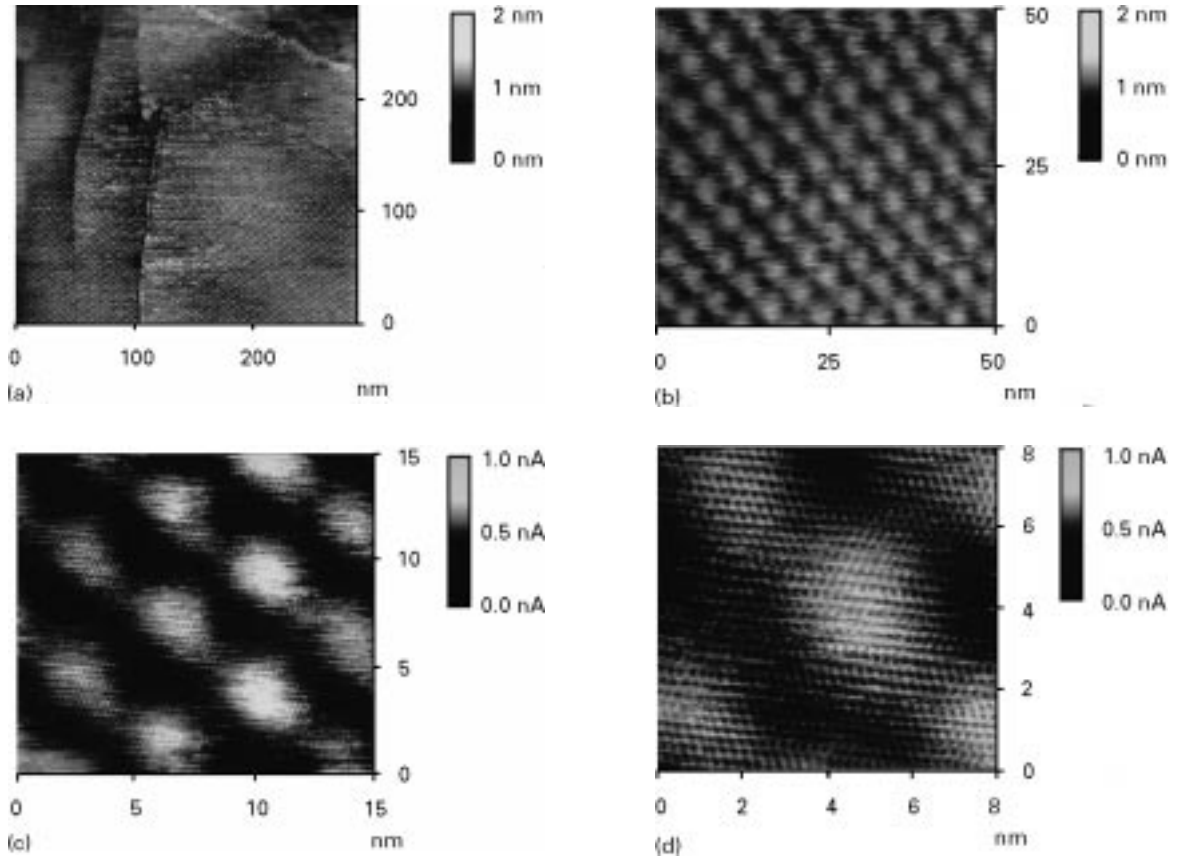

Figure 4 STM images of one region on sample B. Setpoint: 1.04 nA; bias: 51.43 mV. (a) $289 \times 289\,nm^2$ (height mode) Z range: 2 nm; scan rate: 2.98 HZ. Note the smooth surface on the top right-hand corner. (b) $50 \times 50\,nm^2$ (height mode). Z range: 2 nm; scan rate: 7.18 Hz. (c) $15 \times 15\,nm^2$ (current mode). Z range: 1 nA; scan rate: 40.69 Hz. (d) $8 \times 8\,nm^2$ (current mode). Z range: 1 nA; scan rate: 61 Hz.

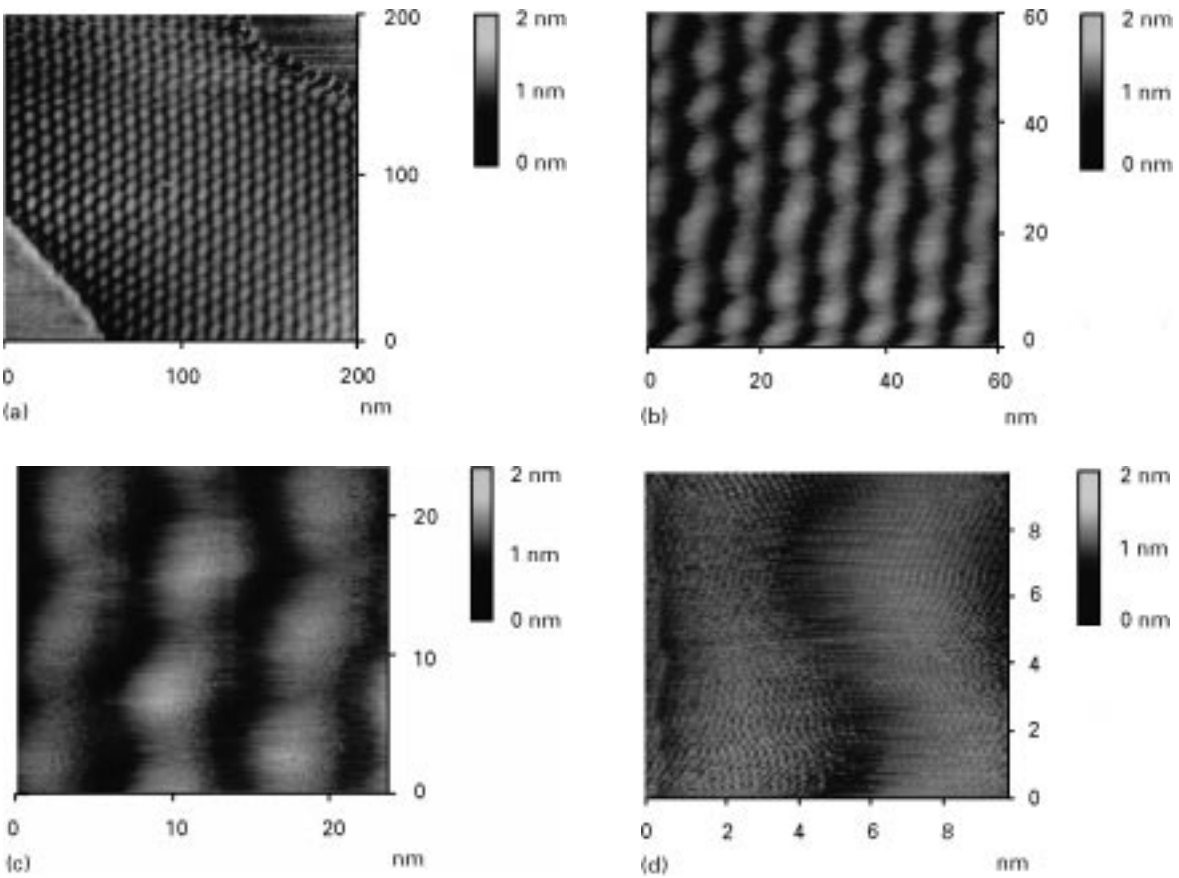

Figure 5 Height mode STM images of another region on sample B. Z range: 2 nm; scan rate: 1.81 nA; bias: 56.63 mV. (a) $200 \times 200\,nm^2$ (1.65 Hz). (b) $60 \times 60\ nm^2$ (1.88 Hz). (c) $20 \times 20\,nm^2$ (4.69 Hz). (d) $10 \times 10\,nm^2$ (5.81 Hz). The values in parentheses are scan rates.

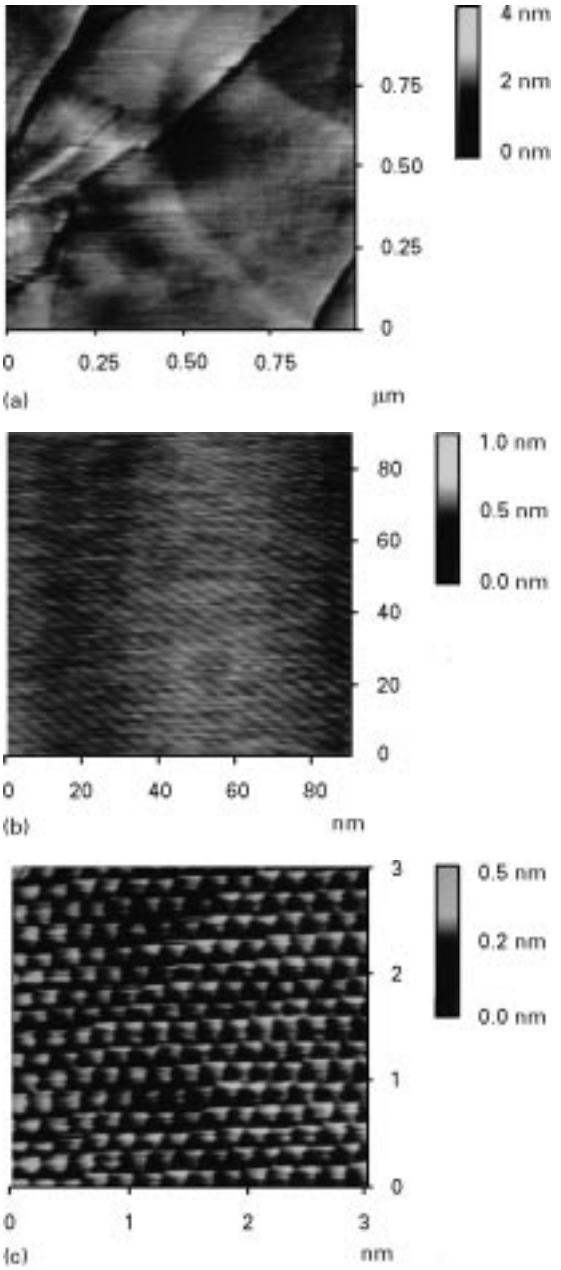

Figure 6 AFM images for sample B. Setpoint: -5 V. (a) $1000 \times 1000\,nm^2$ (height mode) with scan head J Z range: 4 nm; scan rate; 1.06 Hz. (b) $90 \times 90\,nm^2$ (height mode) with scan head A scan rate: 6.14 Hz. (c) $3 \times 3\,nm^2$ (deflection mode) with scan head A: Z 0.5 nm; scan rate: 40.69 Hz. Note the brightness contrast of the wave peaks and valleys.

AFM image. There seems to be a two-dimensional wave feature in the right-hand part of this figure, though it is not very clear. Fig. 6b shows rows of lines with a periodicity of 2.6 nm. The deflection mode was used to obtain an AFM image with the highest magnification (of part of the same region as in Fig. 6b) as shown in Fig. 6c. The corrugation of the waves is very small, so that the wave peaks are seen as brighter areas with wave valleys as darker areas. The graphite atomic lattice can also be seen, with the amplitude of the corrugation larger than that of the anomalous wave contrast. This is similar to the charge density wave (CDW) pattern on tantalum disulfide ($1T$–T_aS_2), which shows larger contrast than the atomic corrugation for STM observations and vice versa for AFM observations [20, 21]. No such features were found by SEM possibly because of the limitation of the SEM's vertical resolution.

4. Discussion

In comparison with ion bombardment, the electron penetrates the target much more deeply due to the very low mass. For simplicity, the average range, R, of 1.8 MeV electrons (at a normal incident angle) is calculated by the following empirical formula [22]

$$R = 0.542E_e - 0.133 = 0.542 \times 1.8 - 0.133$$

$$= 0.8426\,g\,cm^{-2} = 0.32\,cm$$

while the density for graphite is 2.62 $g\,cm^{-3}$. The effects of electrons are in the bulk. That is the reason why the graphite surface remained the same as the original atomic lattice for electron irradiation with doses up to $10^{16}\,e^-\,cm^{-2}$ at incident angle of 45° (samples C and D).

At grazing incidence, interaction of the electrons with the target is in the near-surface region. The maximum energy, T_{max}, transferred by an electron to a carbon atom is given by simple calculation [23]

$$T_{max} \approx 2E_e(E_e + 2m_ec^2)/M_cc^2$$

$$= 2 \times 1.8\,MeV(1.8\,MeV + 2 \times 0.511\,MeV)/$$

$$(12 \times 1836 \times 0.511\,MeV) = 0.9\,KeV,$$

which is high enough to displace the lattice atoms. At a low dose of $5 \times 10^{12}\,e^-\,cm^{-2}$ the area density of electrons arriving at the tilted surface should be reduced by $1/\cos(86°) = 14.3$, a single electron–carbon interaction is proposed to be the mechanism that produces some vacancies and interstitials in the layers just below the surface, in a way similar to single ion impacts [1–18]. At room temperature (approximately 300 K), vacancy migration and agglomeration does not occur, while interstitial carbon atoms in the undisturbed HOPG are mobile and tend to migrate in the region between the close packed planes to form clusters between the planes, therefore forming nanometre-scale hillocks in the surface planes as observed for sample A. The difference from single ion impacts is that the density of the nanometre-size features is much less than that of electrons arriving at the surface, unlike the case for ion bombardment. This difference can be attributed to the fact that there is a lower probability of collision resulting in atomic displacements close to the surface in the case of electron bombardment. The "pearl-necklace" effect (the chain of hillocks in Fig. 2d) appears to be due to a cascade generated by a primary knock-on carbon atom creating a row of interstitials immediately below the surface layer.

For the high dose of $5 \times 10^{14}e^-\,cm^{-2}$ (near grazing incidence), it was amazing for us at first to observe the anomalously large superperiodicity (or two-dimensional wave) superimposed on the normal atomic spacing of graphite, which is surprisingly similar to the features reported for cleaved HOPG surfaces [24, 25].

It has been suggested [24, 25] that the observed superperiodicity is a rotational Moiré pattern due to the presence of a misoriented layer. These features were found by chance and no explanation of their origin was put forward. In our experiment, these features are observed for a HOPG surface modified by 1.8 MeV electron irradiation with a dose of 5×10^{14} $e^- cm^{-2}$ at 86° incidence. Before irradiation, this sample (B) together with the others (A, C and D) was checked and showed no such features. These features only appeared after irradiation for sample B (and not for any of the others). As in [24], the expression

$$D = d/(2 \sin\theta/2)$$

where (D is the period of a rotational Moiré pattern, and d the spacing of the misoriented lattices) was used here to calculate the misorientation angle, θ. It was found that the theoretical estimates are consistent with the results in our experiment reasonably well. We believe that these features are also Moiré patterns as suggested by [24], and are due to the effects of electron bombardment at grazing incident angle. As discussed above, for 5×10^{12} $e^- cm^{-2}$ at 86°, defects of nanometre-size hillocks are formed by interstitial carbon atoms due to single electron–carbon interaction. At the higher dose of 5×10^{14} $e^- cm^{-2}$ (100 times higher than the former) at 86°, the structures and microstructures of the graphite surface are expected to evolve under irradiation. Transmission electron microscope (TEM) studies [26, 27] for electron irradiated HOPG [300 KeV, up to five displacements per atom (d.p.a.) or 5.5×10^{24} $e^- cm^{-2}$] have shown the absence of long-range order in the basal plane, with lattice fringes broken to small segments of 0.5–5 nm in length. It has been proposed [26, 27] that the interstitial atoms and clusters produced by electron irradiation fracture the lattice into fragments that readily rotate by a small angle from their original plane orientation due to weak van de Waals' interaction between graphite layers. In our experiment with much lower dose, the fragmentation should be minor, which means the dimension of the fragments from the break-up of the surface layers is larger (up to hundreds of nanometres) and the fragments largely retain six-fold atomic rings. We suggest that the overlay between misoriented fragments of surface layers and the underlying single crystal results in the Moiré-like superperiodicity observed in our experiment. In the meantime, this experiment seems to verify the hypothesis of the presence of misoriented layers in [24, 25]. Structural changes at the boundary are attributed to valence electrons from the broken carbon–carbon bonds at the edges of fragments.

It is still plausible to explain the non-uniformity of the wave features compared with irradiation using the scanning method. This is possibly due to the rough topography of the graphite surface, with high steps on a large-scale size, and the non-uniformity of the irradiation at gazing incident angle.

AFM observations also show these features with a lower amplitude of corrugation. It seems that the superperiodicity is both electronic and topographic in origin, with the former of more importance.

5. Conclusions

HOPG surfaces irradiated by 1.8 MeV electrons have been observed using SPM. For doses up to 10^{16} $e^- cm^{-2}$ at 45° incident angle, the surfaces remained the same as the original samples, showing flat terraces on a large scale and normal atomic lattices with periodicity of 0.246 nm at highest magnification. It is supposed that the evolution of structures and microstructures under irradiation are in the bulk sample and therefore hardly observed on the surface. For near-grazing incidence with a dose of 5×10^{12} $e^- cm^{-2}$, nanometre-size hillocks are observed, some elongated along the direction of the incidence beam. These are attributed to the effects of single electron–carbon interactions in the top surface layers. At a dose of 5×10^{14} $e^- cm^{-2}$ (at the grazing incident angle,) both STM and AFM observations show an anomalously large (period 2.5–17 nm) superperiodicity (an approximately hexagonal two-dimensional wave) superimposed on the usual 0.246 nm atomic spacing of graphite. The Morié-like pattern with a rotational misorientation angle of 0.6–5° suggests the corrugations are electronic as well as topographic in origin. We propose that near grazing incident electron bombardment with a dose of 5×10^{14} $e^- cm^{-2}$ causes break-up of the surface layers into fragments (hundreds of nanometres in dimension), largely retaining six-fold atomic rings, that rotate by a small angle resulting in the observed features, by overlaying with the underlying single crystal layers. Other properties, such as the valance electrons from the broken carbon–carbon bonds at edges, account for the observation of considerable distortions. Further systematic studies on electron–neutron–proton irradiated HOPG surfaces are underway.

Acknowledgements

This work was supported in part by the Research Grants Committee of the Hong Kong University Grant Council and the Open Laboratory of "Irradiation Physics and Technology" of the state Education Commission of the People's Republic of China. The use of the electrostatic electron accelerator in Sichuan University (People's Republic of China) is gratefully acknowledged. We are also indebted to Mr Chiu Wai kit (Department of Physics, the Chinese University of Hong Kong) for his capable assistance with SEM.

References

1. L. PORTE, M. PHANER, C. H. DE VILLENEUVE, N. MONCOFFRE and J. TOUSSET, *Nucl. Instru. Methods Phy. Res.* **B44** (1989) 116.
2. L. PORTE, C. H. DE VILLENEUVE and M. PHANER, *J. Vac. Sci. Techol.* **B9**(2) (1991) 1064.
3. R. CORATGER, A. CLAVERIE, F. AJUSTRON and J. BEAUVILLAIN, *Surf. Sci.* **227** (1990) 7.
4. R. CORATGER, A. CLAVERIE, A. CHAHBOUN, V. LANDRY, F. AJUSTRON and J. BEAUVILLAIN, *ibid.* **262** (1992) 208.
5. H. KANG, K. H. PARK, C. KIM, B. S. SHIM, S. KIM and D. W. MOON, *Nucl. Instru. & Methods Phys. Res.* **B67** (1992) 312.

6. G. M. SHEDD and P. E. RUSSELL, *J. Vac. Sci. Technol.* **A9**(3) (1991) 1261.
7. T. C. SHEN, R. T. BROCKENBROUGH, J. S. HUBACEK, J. R. TUCHER and J. W. IYDING, *ibid.* **B**(2) (1991) 1376.
8. H. KEMMER, S. GRAFSTROM, M. NEITZER, M. WORTGE, R. NEUMANN, C. TRAUTMANN, J. VETTER and ANGERT, *Ultramicroscopy*, **42**–**44** (1992) 1345.
9. T. LI, B. V. KING, R. J. MACDONALD, G. F. COTTERILL, D. J. O'CONNOR and Q. YANG, *Surf. Sci.* **312** (1994) 399.
10. JUNJUE YAN, ZHIGANG LI, CHUANYONG BAI, W. S. YANG, YUGANG WANG, WEIJIANG ZHAO, YIXIU KANG, F. C. YU, PONGJI ZHAI and XIAOWEI FANG, *J. Appl. Phys.* **75** (3) (1994) 1390.
11. C. MARTON, H. BU, K.J. BOYD, S. S. TODOROV, A. H. AL-BAYATI and J. W. RAVALAIS, *Surf. Sci.* **326** (1995) L489.
12. K. P. REIMANN, W. BOLSE, U. GEYER and K. P. LIEB, *Europhy. Lett.* **30** (8) (1995) 463.
13. W. BOLSE, K. REIMANN, U. GEYER and K. P. LIEB, *Nucl. Instru & Methods* **B,** in press.
14. L. P. BIRO, J. GYULAI and K. HAVANCSAK, *ibid.* in press.
15. A. M. C. PEREZ-MARTIN, J. DOMINGUEZ-VAZQUEZ, J. J. JIMENEZ-RODRIGUEZ, R. COLLINS and A. GRAMARTI, *Nucl. Instru. Methods Phys. Res.* **B90** (1994) 424.
16. J. R. HAHN, H. KANG, S. SONG and I. C. JEON, *Phys. Rev.* **B53** (1996) R1725.
17. Q. YANG, T. LI, B. V. KING and R. J. MACDONALD, *ibid.* **B53** (1996) 3032.
18. C. T. REIMAN, P. A. SULLIVAN, A. TURPITZ, S. ALTMAN, A. P. QUIST, A. BERGMAN, S. O. OSCARSSON, B. U. R. SUNDQVIST and P. HAKANSSON, *Surf. Sci.* **341** (1995) L1019.
19. B. K. ANNIS, D. F. PEDRAZA and S. P. WITHROW, *J. Mater. Res.* **8** (1993) 2587.
20. R. C. BARRETT, J. NOGAMI and C. F. QUATE, *Appl. Phys. Lett.* **57** (1990) 992.
21. C. G. SLOUGH, W. W. MCNAIRY, R. V. COLEMAN, J. GARNAES, C. B. PRATER and P. K. HANSMA, *Phys. Rev.* **B42** (1990) 9255.
22. P. MARMIER and SHELDON, in "*Physics of Nuclei and Particles*", Vol. 1, (Academic Inc, New York, 1969) Ch. 4.
23. A. DUNLOP, F. RULLIER-ALBENQUE, C. JAOUEN, C. TEMPLIER and J. DAVENAS (eds) "*Materials under Irradiation*", (1993) p. 31.
24. M. KUWABARA, D. R. CLARKE and D. A. SMITH, *Appl. Phys. Lett.* **56** (1990) 2396.
25. J. E. BUCHLEY, J. L. WRAGG, H. W. WHITE, A. BRUCKDORFER and D. L. WORCESTER, *J. Vac. Sci. Technol.* **B9** (1991) 1079.
26. J. KOIKE and D. F. PEDRAZA, *Mater. Res. Soc. Symp. Proc.* **279** (1993) 67.
27. *Idem*, *J. Mater. Res.* **9** (1994) 1899.

Received 11 October 1996
and accepted 23 June 1998